Design of artificial membrane transporters from gold nanoparticles with controllable hydrophobicity

Marcin P. Grzelczak, Alexander P. Hill, Domagoj Belic, Dan F. Bradley, Casper Kunstmann-Olsen and Mathias Brust*

Affiliation: *University of Liverpool, Department of Chemistry, Crown Street, Liverpool L69 7ZD*

*Corresponding author: mbrust@liverpool.ac.uk

Abstract: Gold nanoparticles with variable hydrophobicity have been prepared in three different size regimes following established methods. The control of hydrophobicity was achieved by complexation of the 18-crown-6-CH_2-thiolate ligand shell with potassium ions. Potassium dependent phase transfer of these particles from dispersion in water to chloroform was demonstrated, and the equilibrum partitioning of the particles in water-chloroform liquid/liquid systems was quantified by optical spectroscopy. The gradual complexation of the ligand shell with potassium ions was further monitored by zeta potential measurements. Potassium dependent insertion of nanoparticles into the phospholipid bilayer membrane of vesicles in aqueous dispersion has been demonstrated by cryogenic transmission electron microscopy (cryo-TEM). Nanoparticle-dependent potassium ion transport across the vesicle membrane has been established by monitoring the membrane potential with fluorescence spectroscopy using a potential sensitive dye.

Introduction

At a certain level of structural or functional complexity, asymmetry becomes a vital property of the constituents of self-assembled systems.[1] Without delving into theory, this statement is intuitively corroborated by looking at the elemental building blocks of existing assemblies at any scale, not least Lego® bricks, the asymmetry of which forms the basis for their directional assembly. The growth of microtubules, which are part of the cytoskeleton and, among other functions, responsible for directional intracellular transport, represents one of countless biological examples of directional assembly, in this case from bipolar protein subunits.[2] Unlike proteins and other biomolecules, most artificial nano-objects are crystalline groups of atoms, ions or molecules, sometimes protected by a molecular ligand shell and usually highly symmetric. In order to break this symmetry, for example by creating a top and a bottom or a left and a right side, these objects have to interact with an asymmetric environment, which could be an external electric[3,4] or magnetic field,[5,6] directional flow[7] or freezing,[8] any type of gradient, or an interface.[9–12] In this contribution we demonstrate the rational design of water dispersible gold nanoparticles that can be programmed to reside at the interfaces formed by phospholipid bilayer membranes in an aqueous dispersion of vesicles. This is achieved by increasing the hydrophobicity of the particles in a controlled fashion *via* complexation of potassium ions in their ligand shell. The complexing ligand chosen here is a thiolated crown ether, which is known to become more hydrophobic upon complexation of potassium ions.[13] This interaction has been used before to control the hydrophobicity of nanoparticles[14,15] but not to target phospholipid membranes with them. However, crown ethers modified with self-assembling moieties[16,17] and with peptides[18] have been reported to reside in bio-membranes and to act as artificial ion channels. Once our particles were bound to the membrane, we could have tried to take advantage of this environment to modify the particles only on one side creating asymmetry in the ligand shell. There are indeed many reports on similar approaches to this end.[10,11,19] Instead of exploring this route, we were interested in probing the functionality of membrane bound particles and found that they act as specific potassium transporters and, in the presence of a potassium concentration gradient, rapidly polarise the membrane to the corresponding potential. In this discussion article we present the design and preparation of crown ether modified gold nanoparticles of three different sizes, detailed phase transfer studies and zeta potential measurements to demonstrate the control of hydrophobicity by complexation of potassium ions to the crown moieties, and finally vesicle membrane polarisation by membrane bound nanoparticles in the presence of a potassium ion concentration gradient across the membrane.

Experimental

Chemicals

Trisodium citrate $Na_3C_6H_5O_7$, hydrogen tetrachloroaurate (III) hydrate $HAuCl_4 \cdot 3H_2O$, sodium borohydride $NaBH_4$ were supplied by Aldrich. *O*-[2-(3-Mercaptopropionylamino)ethyl]-*O′*-methylpolyethylene glycol (mPEG-SH, Mw 5000) was purchased from Sigma-Aldrich. Liposome kit and LiCl, NaCl, KCl salts were purchased from Sigma. 18-crown-6-CH_2 was supplied by ProChimia. Pure-grade methanol, ethanol and Milli-Q-grade water were used in all preparations.

Synthesis of 2 nm Au/18-C-6-CH_2-SH NPs

Small, 2 nm Au/18-C-6-CH_2-SH NPs were synthesized by a modified literature method[20,21] where a 1:1 Au^{III}: capping agent ratio was used. Briefly, 3 ml of a 9 mM solution of hydrogen tetrachloroaurate (III) hydrate in methanol was mixed with 3 ml of a 9 mM solution of 18-C-6-CH_2-SH in methanol resulting in a clear yellow solution. The mixture was stirred for 10 minutes at room temperature and turned almost colorless and slightly cloudy. Then, 3 ml of a freshly prepared 0.056 M solution of $NaBH_4$ in methanol was rapidly added under vigorous stirring. Upon addition, the solution quickly became deep brown in color and was left for 15 minutes to allow the reaction to proceed to completion. After one hour, the resulting Au/18-C-6-CH_2-SH NPs dispersion was rotary evaporated at 30°C to yield a black residue of NPs which was washed three times with diethyl ether. In the final step, the crude product was redispersed in iso-propanol to remove excess hydrophilic reaction products that were filtered off, and after careful rotary evaporation (30°C) the purified product was obtained as a black solid, which was dispersed in MQ water for further use.

Synthesis of citrate stabilised particles.

Citrate Au NPs were synthesized by a modified Turkevich method reported by Bastús[22] *et al.* Briefly, an aqueous solution of trisodium citrate (2.2 mM, 75 ml) was refluxed for 15 minutes, and aqueous $HAuCl_4$ (0.5 ml, 25 mM) was rapidly added to the solution under vigorous stirring. Over a period of 10 minutes, the colour of the mixture gradually became deeper red. The reaction mixture was left stirring for a further 20 minutes to ensure the reaction had gone to completion and then left to cool to room temperature.

To grow larger particles, the above procedure was repeated but instead of allowing the mixture to cool down, the temperature was reduced to 90 °C, and 1 ml of the dispersion was replaced by 0.5 ml of a trisodium citrate solution (60 mM) and 0.5 ml of an $HAuCl_4$ solution (25 mM). This process was repeated every 4 hours to a total of 4 times. It promoted the gradual growth of particles to a final size of 38 nm.

Two step functionalization of citrate particles with 18-C-6-CH_2-SH

Lack of stability control in direct functionalization of citrate Au NPs with 18-C-6-CH_2-SH led us to introduce an intermediate step which consists of replacing citrate ligand with *O*-[2-(3-Mercaptopropionylamino)ethyl]-*O′*-methylpolyethylene glycol (mPEG-SH, Mw 5000) molecule. This was then followed by ligand replacement in ethanol with a large excess of 18-C-6-CH_2-SH. In order to functionalize Au/citrate NPs with m-PEG-SH 5000 an aqueous dispersion of 15 nm citrate particles (30 ml) was mixed with m-PEG-SH 5000 (4 molecules per nm^2 of total gold NPs surface) under vigorous stirring. The solution was left to stir for 40 minutes at room temperature to ensure complete functionalization occurred. The solution was then centrifuged at 14500 rpm for 30 minutes, followed by the removal of water and re-dispersion in ethanol (5ml); this purification process was repeated 3 times.[23]

In the same way, larger, 38 nm citrate Au particles were functionalized with the same number of m-PEG 5000 molecules per nm^2 based on the total gold NPs surface.

In order to replace the intermediate m-PEG 5000 ligand with the desired one, a solution of 18-C-6-CH_2-SH (400 molecules per nm^2 of total gold NPs surface) dissolved in 1ml of ethanol was slowly added drop wise under vigorous stirring to the ethanolic dispersion of 15 nm Au/m-PEG 5000 NPs (25ml). The mixture was then sonicated for 20 minutes and left at room temperature for 12 hours. The product was isolated by repeated centrifugation at 12000 rpm (1 hour) and re-dispersion in MQ water. Samples were then analysed by TEM and UV-Vis.

The above process was repeated for the larger 38 nm citrate particles with the same number of 18-C-6-CH_2-SH ligand molecules 400 per nm^2.

Phase Transfer of Au/18-C-6-CH_2-SH NPs

Dispersions containing 2 nm Au/18-C-6-CH_2-SH ($(8 \pm 1) \times 10^{14}$ NPs/mL) were mixed with KCl to adjust the following final concentrations of salt in aqueous phases: 0, 1.25, 12.5, 62.5, 200, 400 mM, followed by shaking for 15 seconds. Then each sample was carefully added to chloroform (1 ml) to form a two-phase water/chloroform system in a glass vial (4 ml). Pictures were taken at regular time intervals to monitor the gradual phase transfer of the particle.

Phase transfer experiments with larger particles (15 and 38 nm) were all carried out at a constant KCl concentration of 4 mM. The concentrations of particles were adjusted to give comparable optical densities.

The phase transfer ability of different cations (LiCl, NaCl and KCl) was tested with 2 nm particles ($(8 \pm 1) \times 10^{14}$ Au/18-C-6-CH_2-SH NPs/mL); experiments were performed as described above.

Quantitative particle partitioning experiments were carried out in the same way except for the rapid equilibration, which was achieved by vortexing the two-phase systems for 10 s. After phase separation, samples were analysed by UV-Vis.

Zeta Potential Measurements

All measurement were carried out with a Malvern zetasizer nano ZSP. For this purpose, KCl was added to aqueous dispersions containing 2nm Au/18-C-6-CH_2-SH ($(3 \pm 0.5) \times 10^{11}$ NPs/mL) to the following final salt concentrations: 0, 0.25, 2.5, 8, 12.5, 20, 30, 40 μM.

TEM and HRTEM

TEM samples were prepared by drop casting 3 μl of Au nanoparticle colloidal solution onto holey carbon TEM grids (Agar Scientific or TAAB). After drying in air, the samples were imaged on an FEI Tecnai Spirit G2 BioTWIN TEM at an accelerating voltage of 120 kV, using an Olympus-SIS MegaView III digital camera. High-resolution TEM was performed on an aberration-corrected JEOL JEM 2100FCs microscope operating in STEM mode at an accelerating voltage of 200 kV.

Vesicles preparation

Vesicles were prepared by a modified variant of the method described by Newcomb[24] *et al*. Briefly, a 10 mM stock solution of phospholipids was made by dilution of liposome kit lyophilized powder (Cholesterol 9 μmol, L-α-Phosphatidylcholine (egg yolk) 63 μmol, Stearylamine 18 μmol) in chloroform. 1 ml aliquots of the stock solution were rotary evaporated for 2 hours in order to remove all residues of organic solvent. MQ water or KCl and NaCl buffer solutions were used to hydrate the phospholipids depending on the requirements of each experiment. In order to make the white suspension of phospholipids more homogeneous, it was heated to 60˚C followed by 4-5 freeze thaw cycles using liquid nitrogen. Next, the hydrated and homogeneous phospholipid solution was extruded 20 times through a mini-extruder (Avanti) with a 100-nm-pore-size polycarbonate filter (Whatman) to form vesicles of about 100 nm diameter. The vesicle dispersion was purified by dialysis using MWCO 12000-14000 dialysis tubing (Serva).

Cryo-TEM

Samples for cryo-TEM were prepared by dropcasting 4 μL of the solution onto freshly glow-discharged holey carbon TEM grids (Agar Scientific or TAAB). After 60 s of incubation, the grids were double-side blotted for 2×2 s and plunge-frozen using an FEI Vitrobot Mk2 system working at >96% relative humidity. Vitrified samples were transferred onto a 626 Gatan cryo-holder and imaged on the FEI Tecnai Spirit G2 BioTWIN TEM in low-dose mode at an accelerating voltage of 120 kV.

Membrane potential changes detected by fluorescence spectroscopy

The suspension of vesicles with a final concentration of phospholipids of 1 mM was placed in a fluorimetric cuvette followed by addition of the potential probe dye Safranin O (180 nM final concentration). Then the fluorescence intensity was allowed to equilibrate for 2 minutes. The kinetic mode was used to detect continuously fluorescent intensity changes at 589 nm with an excitation wavelength of 521 nm.

Next, 20 nM of valinomycin or different concentrations of 2 nm Au/18-C-6-CH_2-SH NPs was added, and the fluorescence intensity was monitored for 1700 s.

Results and Discussion:

A modified capping agent, 18-C-6-CH_2-SH, which is a thiol-derivative of a crown ether (18-crown-6) was immobilized on the gold particle surface by binding via its thiol functionality as illustrated in Figure 1a. Gold nanoparticles of three different size regimes, around 2, 15 and 38 nm were prepared and modified in this way. The corresponding TEM or HRTEM images, size distributions and UV-Vis spectra are shown in Figure 1. The differences in size are clearly manifested in the evolution of the UV-Vis spectra (Figure 1b). The smallest NPs show virtually no plasmon peak (black line) whereas the largest exhibit a pronounced and slightly red shifted plasmon band (red line).

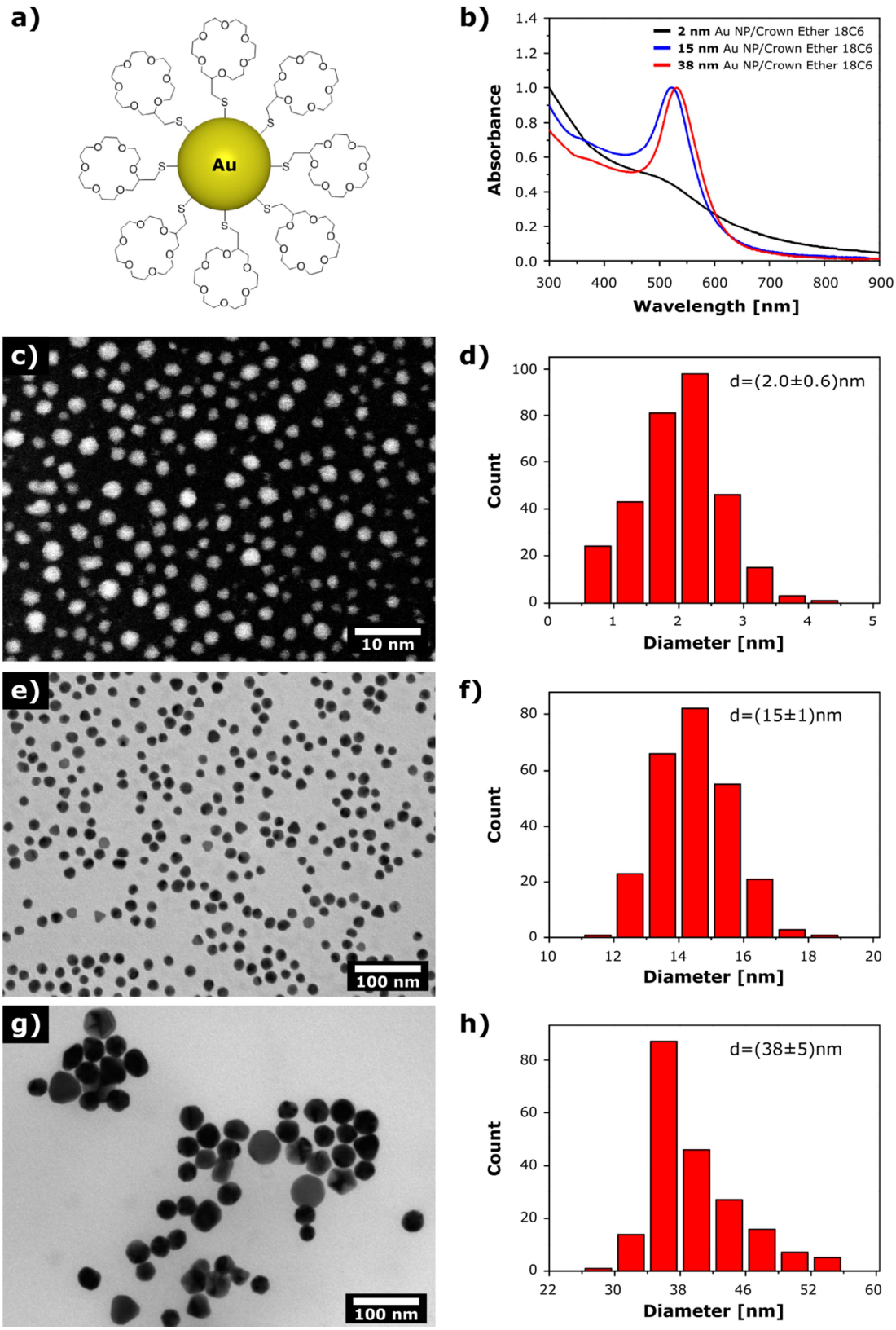

Figure 1. (a) Model of Au NP functionalized with crown ether 18-C-6-CH_2-SH. (b) UV-Vis spectra of three different sizes of Au/18-C-6-CH_2-SH NPs in water. (c) High angle annular dark field (HAADF) STEM image of 2 nm Au/18-C-6-CH_2-SH NPs. (e, g) Bright field TEM images of 15 nm and 38 nm Au/18-C-6-CH_2-SH. (d, f, h) The corresponding size distributions.

The idea of using crown ether 18-crown-6 as capping agent is based on its well established complexation-dependent hydrophobicity. The hydrophilic ethylene oxide ring becomes much more hydrophobic upon complexation of cations, in particular potassium, which binds very strongly to the cavity. The strategy of controlling the hydrophobicity of supramolecular objects in this way has been reported several times.[25,26] Recently M. I. Bodnarchuk[15] *et al.* have shown that the presence of macrocyclic ethers enables the solubilization of inorganic- capped NPs in solvents of any polarity and improves an ability to form NP superlattices. Since our gold NPs are functionalized with 18-crown-6 molecules which are capable of selectively coordinating hard alkali metal ions such as potassium[27,28] the solubility of those NPs in different solvents can be tuned by changing type and salt concentration in the surrounding medium. This is confirmed by the simple experiment shown in Figure 2, where the same concentration of the 2 nm Au/18-C-6-CH_2-SH NPs dispersed in water was brought in contact with a chloroform phase. In this way, two immiscible phases were created with the well-defined interface. The only variable component in each vial presented in Figure 2 is the KCl salt concentration. In figure 2a the initial and the final state of phase transfer after 18 hours are shown indicating that even after a long time equilibrium has not yet been reached. A more detailed time evolution of this process is presented in Figure S1. Both the absence and much higher concentrations of KCl salt either entirely preventing, or dramatically slowing down the phase transfer process.

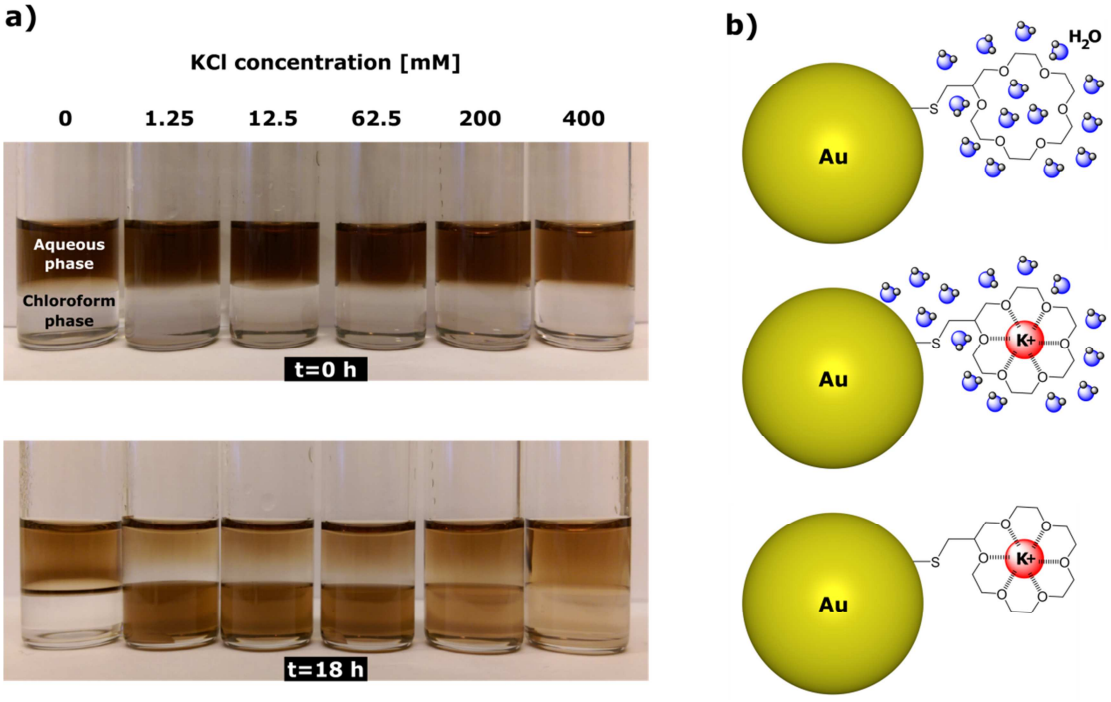

Figure 2. (a) Photos of phase transfer experiments from water to chloroform of 2 nm Au/18-C-6-CH_2-SH NPs at different KCl salt concentrations. (b) Model of hydrophobicity change upon complexation of potassium ions.

Before complexation, the crown ether 18-crown-6 and hence the Au/18-C-6-CH_2-SH NPs are stable in aqueous media. This is attributable to the oxygen atoms present within the ring (Figure 2a). These are capable of hydrogen bonding with water molecules resulting in an energetically favorable process for the water to form a solvent shell around the 18-Crown-6-CH_2-SH and hence render the particles dispersible in water.

On the other hand, upon complexation with a suitable cation, the electrons of the oxygen atoms are no longer interacting with the water present in the system but with the complexed cation.[29] This results in the aqueous solvent shell being no longer energetically favorable, and thus in the transfer of the particles to the chloroform phase. The data shown so far, are qualitative kinetic data of phase transfer, which may not necessarily relate to the thermodynamic properties of the system. For this reason, we have also looked at the equilibrium partition of NPs between the water and the chloroform phase. NPs were first dispersed in water and in aqueous KCl solutions in the same concentration range used in Figure 2a and then thoroughly vortexed together with a chloroform phase. After this, when phase separation had completed (Figure 3a, b), UV-Vis spectra were taken of both phases to determine the amount of NPs present in both solutions (see Figure S2).

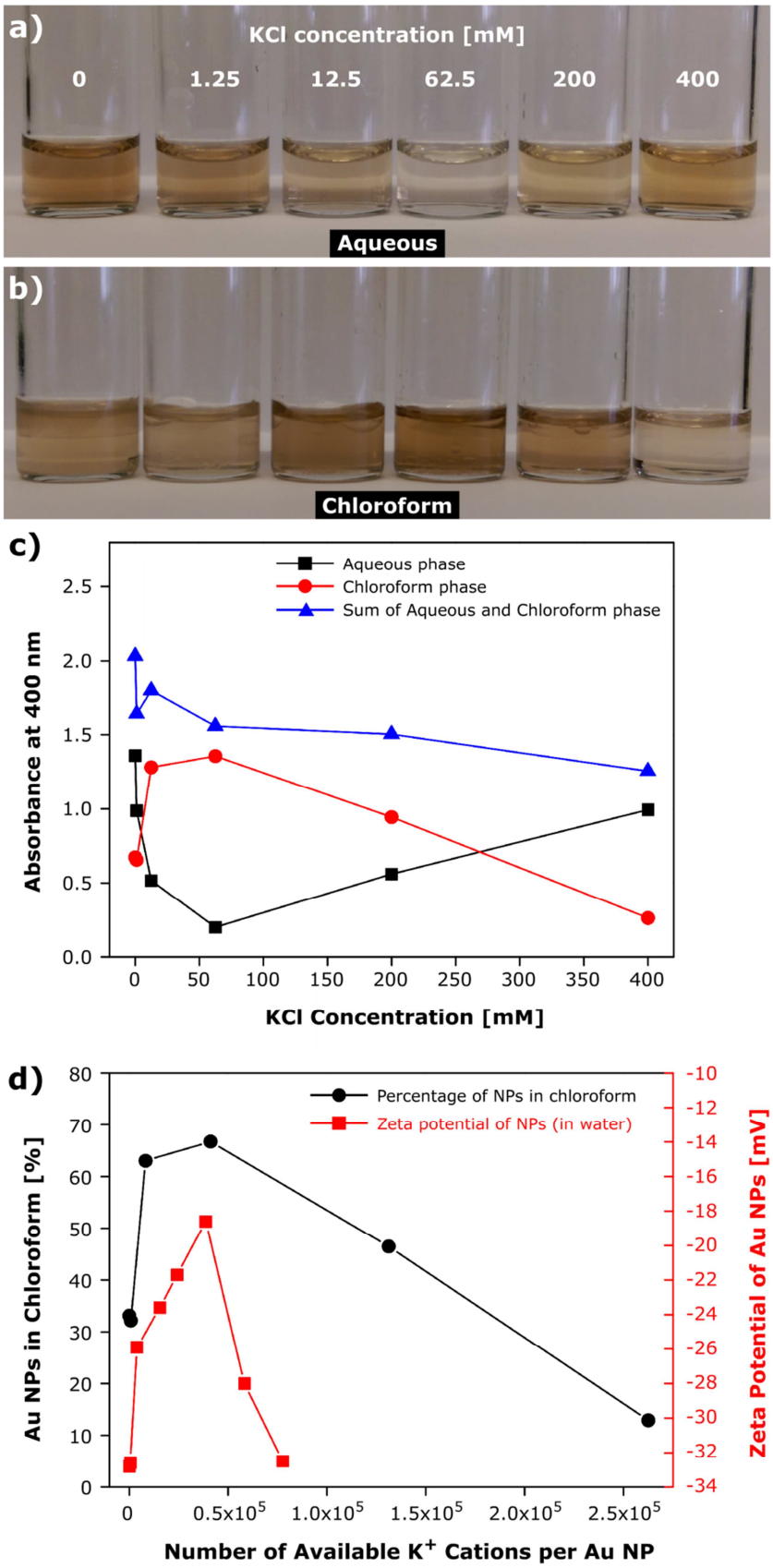

Figure 3. (a), (b) Equilibrium partitioning of 2 nm Au/18-C-6-CH_2-SH NPs in water and chloroform phases after vortexing and solvent separation. (c) Partitioning as a function of salt concentration. (d) Partitioning (only chloroform phase shown) and zeta potential of the particles as a function of the potassium per nanoparticle ratio.

Figure 3a-c shows the equilibrium partitioning of 2 nm nanoparticles between water and chloroform at different potassium chloride concentrations in the aqueous phase, after intense mixing (vortex) and subsequent phase separation. With increasing salt concentration the particles initially become more hydrophobic, reaching maximal hydrophobicity at around 60 mM salt concentration. At further increasing salt concentration this trend is reversed so that at the highest salt concentration used (400 mM) most particles remain in the aqueous phase, comparable to the situation without salt. Thus the empirical optimum of salt concentration for creating hydrophobic particles is at around 60 mM. As we assume that the complexation of potassium ions with the crown ether controls the hydrophobicity of the particles, we have also measured their zeta-potential, which should become more positive with increasing complexation. Unfortunately, the range of salt concentrations of the partitioning experiments (Figure 3a-c) extends by three orders of magnitude the range in which zeta potential measurements are reliably possible (see Figure S3) due to the adverse effect of increased solution conductivity. It is however possible, to conduct zeta potential measurements at relatively low particle concentrations compared to the concentrations typically needed for the partitioning experiments. Therefore we can plot both the zeta potential and the partitioning data on the same graph if we use as the X-axis the ratio between the number of potassium ions and the number of particles present in solution, instead of the salt concentration. This is shown in Figure 3d suggesting indeed a good correlation between the zeta potential and the hydrophobicity of the particles. This notion however has to be regarded with some caution since it implicitly contains the hypothesis that not the absolute salt concentration but the relative amount of salt compared to the number of crown ether moieties matters in determining the hydrophobicity of the particles. We have not yet been able to show unequivocally that this is the case. For example, a change in particle concentration should give a rather different appearance to the graph in Figure 3c since at lower/higher particle concentration, saturation of the crown ether with potassium ions will occur at lower/higher salt concentrations. So far, we found that this is not really the case over the entire range of salt concentrations shown in Figure 3c. Note that the increase in hydrophobicity is initially very steep (between 0 and 10 mM KCl). It appears from preliminary studies that this becomes even steeper at lower particle concentration confirming the model of crown ether saturation with potassium ions. For the nanoparticles used here we would expect no more 300 ligands per particle which means that full saturation with potassium ions maybe expected already at very low potassium concentrations depending to what extend their binding constant is influenced by the confinement of ligands to the nanoparticle surface. Above 10 mM KCl concentration the appearance of the graph is quite independent of particle concentration suggesting an important role of other effects that are independent of particle concentration, for example, the ionic strength of the solution, which can lead to a well-known salting out effect. The most curious behavior is that at higher salt concentrations the hydrophilicity of the particles returns. This may be for the same reason we observe a return of the zeta potential to more negative values bearing in mind the above mentioned limitation that zeta potentials could only be measured at

very low absolute salt concentrations. We tentatively attribute the reverse trends in both the hydrophobicity, and the zeta potential to the build-up of the electrochemical double layer around the nanoparticles which leads increasingly to a screening of the positive charge associated with the complexed potassium ions. From our current understanding we thus consider that three different phenomena cooperate in determining the partition of nanoparticles between water and chloroform. (i) The complexation of potassium ions causing hydrophobicity and lowering the absolute value of the zeta potential, and (ii) the build-up of the electrochemical double-layer causing hydrophilicity and increasing the absolute value of the zeta potential, depend on the potassium/nanoparticle ratio. (iii) The salting out phenomenon, effectively increasing the hydrophobicity of the particles, only depends on the ionic strength of the solution and does not scale with nanoparticle concentration. This is most likely responsible for the significant broadening of the partitioning graph in Figure 3d in comparison with the rather sharply decreasing and increasing curve of the zeta potential. While above 60 mM salt concentration the particles become rapidly more hydrophilic with further increasing salt concentration, the salting out effect works in the opposite direction but is overcompensated eventually.

We have also qualitatively compared phase transfer of crown ether modified gold nanoparticles of three different sizes, 2, 15 and 38 nm. The results are shown in Figure 4a. Particles of all sizes transfer to the organic phase. In all cases, phase transfer is fast compared to diffusion, which leads to depletion of particles in the aqueous phase just above the interface. Even after 23 hours equilibrium is not reached due to the very slow diffusion rate. The UV-Vis spectra taken from the both phases show that the particles remain stable and that there is virtually no loss of particles. Plasmon peaks of 15 and 38 nm Au/18-C-6-CH_2-SH NPs are red shifted in comparison to the absorbance of Au NPs in the aqueous phase what is attributed to changes in the refractive index of the medium.[30]
The small inset in each absorbance spectrum shows the organic phase, which was separated from the bottom of each vial to indicate that NPs are really moving through the interface and are not adhering to the glass wall.

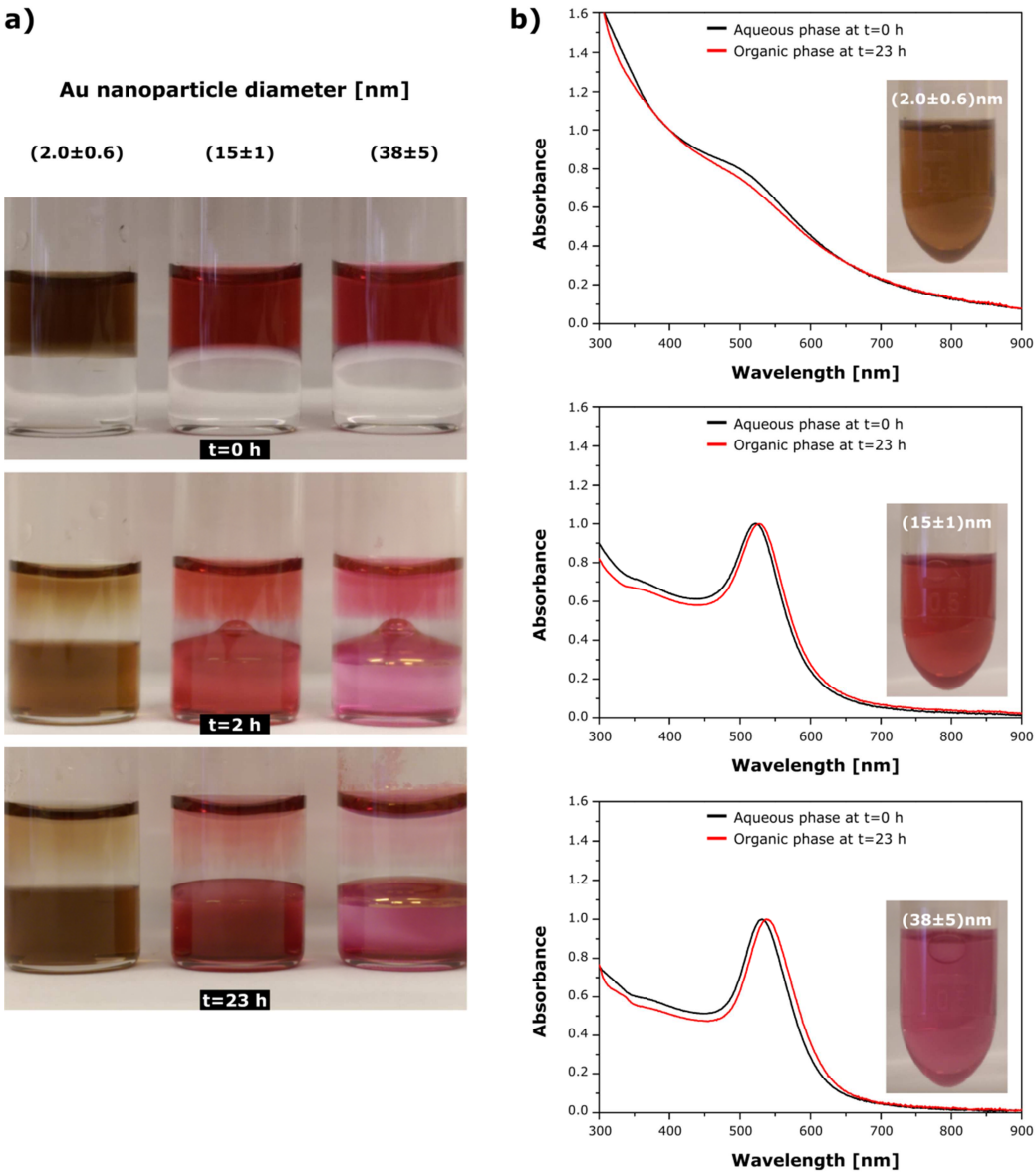

Figure 4. (a) Photos of phase transfer experiments from water to chloroform of three different sizes of Au/18-C-6-CH_2-SH NPs at the same salt concentrations. (b) UV-Vis spectra of the initial aqueous phase and final chloroform phase, for each NP size. The insets show the respective organic phase evidencing fully dispersed and stable nanoparticles.

Having established the ability to control their hydrophobicity, the Au/18-C-6-CH_2-SH NPs were now tested for membrane targeting. For this purpose, unilamellar, positively charged vesicles (zeta potential = 36.5 ± 1.0 mV) were prepared in the absence of salt buffers. Nanoparticles dispersed in a 4 mM aqueous KCl solution and added to the same volume of an aqueous dispersion of vesicles expecting that under these conditions the particles are fully complexed with potassium and hence sufficiently hydrophobic to associate preferentially with the vesicle membrane. After 60 min of incubation samples were prepared for inspection by cryo-TEM. As expected, good adhesion of particles to the vesicles was found (Figure 5 c,d). For comparison, control experiments without KCl shown in Figure 5 a,b gave no evidence for interaction of particles with vesicles.

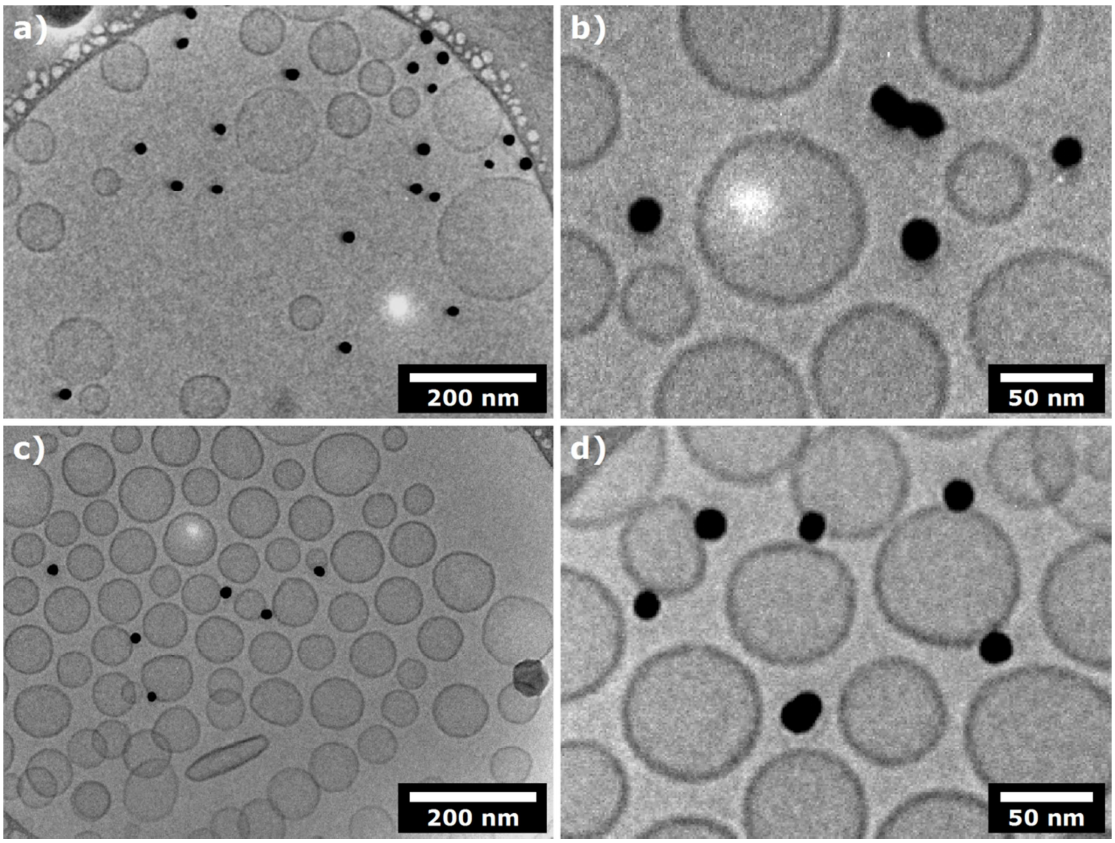

Figure 5. Cryo-TEM images of phospholipid vesicles incubated with 15 nm Au/18-C-6-CH_2-SH NPs for one hour. (a, b) In the absence of K^+ cations the NPs do not get embedded within the vesicle membrane. (c, d) In the presence of 2 mM K^+ cations the NPs exhibit a tendency to associate with the vesicle membrane.

Finally, the high selectivity of 18-crown-6 molecules for potassium allowed us to design experiments where NPs could be used as a new type of artificial ionophore polarizing the phospholipid bilayer membrane of the vesicles. For this purpose, we have adjusted the potassium concentrations inside and outside the vesicles so that in the presence of an ionophore specific for potassium a membrane potential, ψ, is established according to the Nernst Donnan equation.[31]

$$\Delta\psi = \frac{RT}{zF}\ ln\left(\frac{[K^+]_{out}}{[K^+]_{in}}\right) \quad (1)$$

The membrane potential was interrogated by fluorescence spectroscopy using Safranin O as an indicator dye. The fluorescence intensity of this dye depends nearly linearly on the membrane potential (see supporting information Figure S4). The dye is only sensitive if the polarity of the vesicle membrane is inside negative. It is generally assumed that the positively charged dye is driven into the membrane from outside the vesicle by the electric field across the membrane. The results are shown in figure 6. If the potassium concentration is high inside and low outside (Figure 6a) the polarity of the membrane is inside negative and hence membrane potential can be quantified by the fluorescence intensity increase. While the final membrane potential is given by the

Nernst Donnan equation and should not depend on the concentration of ionophore the speed of membrane polarization is expected to depend on the amount of ionophore present. This can indeed be clearly seen in figure 6c where three different concentrations of nanoparticles are compared. For comparison the membrane was also polarised using the well-established ionophore valinomycin. In the case of addition of gold nanoparticles, a small and immediate irreversible drop of fluorescent intensity was observed (for clarity, not shown in Figure 6) that we attribute to quenching by the metal. Otherwise the behavior of valinomycin and gold nanoparticles was near identical. As expected reversing polarity[32] of the membrane potential (Figure 6 b, d) by adjusting high potassium concentration outside of vesicles does not lead to measurable polarization due to the above mentioned limitations of Safranin O. This experiment establishes high selectivity for potassium compared to sodium. The same selectivity can be found in phase transfer experiments, where neither sodium nor lithium is capable of increasing the hydrophobicity of nanoparticles (see Figure S5).

It is somewhat surprising that our particles appear to act as perfect and selective ionophores comparable to the standard compound valinomycin. The mechanism of ion transfer has not been studied and remains open to speculation. It is most likely that the complex potassium is in relatively fast equilibrium with free potassium and that the transfer of potassium across the membrane is facilitated by a tumbling motion of the particles that randomly exposes crown ether moieties to either side of the membrane. An alternative, perhaps even more appealing mechanism could be that the crowns self-organize on the surface of the particle in such a way that a continuous channel is formed. A comparatively high level of ligand shell organization has been reported before in contributions by Rotello *et al.*[33] and by Stellacci *et al.*[34–36] but the latter's have later been disputed by others.[37,38]

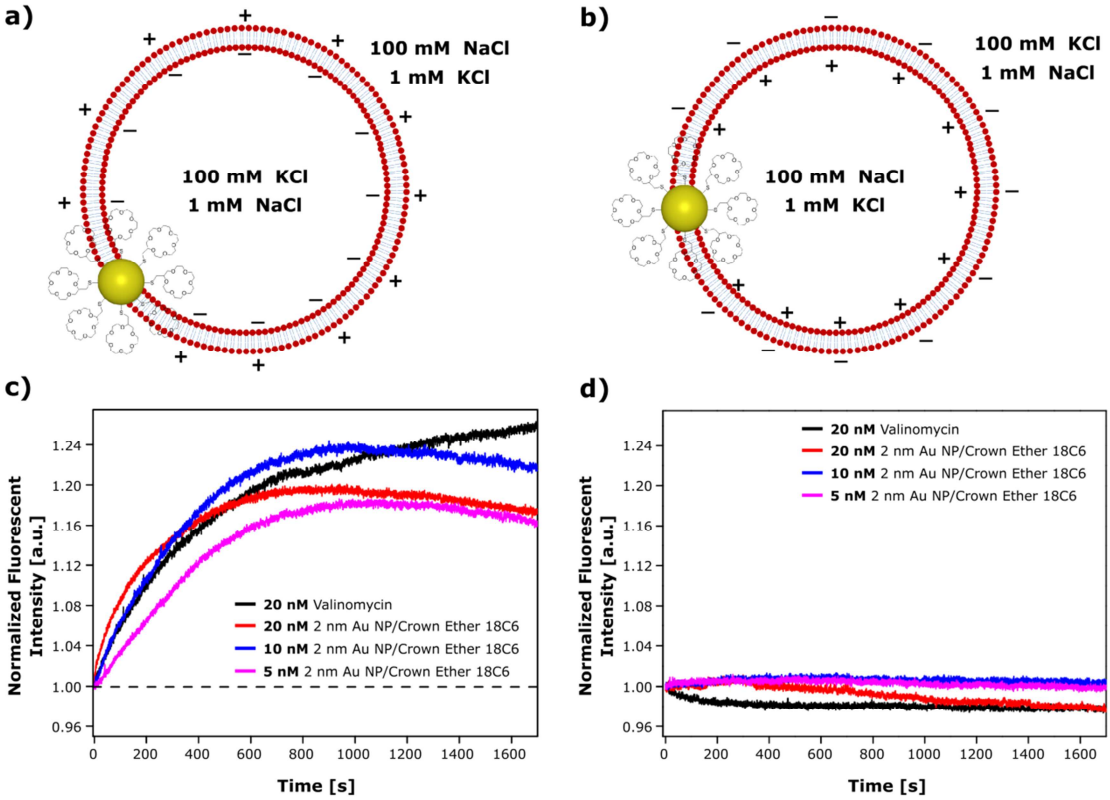

Figure 6. (a, b) Models of polarised phospholipid bilayer membrane. Note that the membrane polarity is determined only by external internal potassium ion concentrations. (c) Normalized fluorescent intensity changes caused by membrane polarization after addition of different concentrations of 2 nm Au/18-C-6-CH_2-SH NPs and, for comparison, valinomycin. (d) Opposite polarization of the membrane dose not lead to fluorescence increase due to the nature of Safranin O.

Conclusions

We have demonstrated a rational approach to the design of gold nanoparticles with controllable hydrophobicity. These particles readily transferred from aqueous to organic dispersion and were successfully employed to target vesicle membranes in an aqueous dispersion as evidenced by cryo-TEM. The particles do not only associate, as expected, with the hydrophobic vesicle membrane, but also act as highly efficient and selective ionophores for potassium ions. Membrane polarization by potassium transfer has been achieved. This report establishes functionalized metal nanoparticles as a new class of membrane transporters with potential applications in sensing and biomedical research.

Acknowledgments

We would like to thank A. Beckett and I. Prior from Biomedical Electron Microscopy Unit, University of Liverpool, and T. Heil and S. Romani from Nanoinvestigation Centre, University of Liverpool. The research was founded through ERC Advanced Grant “PANDORA” under grant number 108269.

References:

(1) Whitesides, G. M.; Boncheva, M. Beyond Molecules: Self-Assembly of Mesoscopic and Macroscopic Components. *Proc. Natl. Acad. Sci. U. S. A.* **2002**, *99* (8), 4769–4774.

(2) Conde, C.; Cáceres, A. Microtubule Assembly, Organization and Dynamics in Axons and Dendrites. *Nat. Rev. Neurosci.* **2009**, *10* (5), 319–332.

(3) Kleinert, J.; Kim, S.; Velev, O. D. Electric-Field-Assisted Convective Assembly of Colloidal Crystal Coatings. *Langmuir* **2010**, *26* (12), 10380–10385.

(4) Ryan, K.M.; Mastroianni, A.; Stancil, K.A.; Liu, H and Alivisatos, A. P. Electric-Field-Assisted Assembly of Perpendiculary Oriented Nanorod Superlattice. *Nano Lett.* **2006**, *6*, 1479–1482.

(5) Ngo, A. T.; Pileni, M. P. Assemblies of Ferrite Nanocrystals: Partial Orientation of the Easy Magnetic Axes. *J. Phys. Chem. B* **2001**, *105* (1), 53–58.

(6) Correa-Duarte, M. A.; Grzelczak, M.; Veronica Salgueiriño-Maceira; Giersig, M.; Liz-Marzán, L. M.; Farle, M.; Sierazdki, K.; Diaz, R. Alignment of Carbon Nanotubes under Low Magnetic Fields through Attachment of Magnetic Nanoparticles. *J. Phys. Chem. B* **2005**, *109*, 19060–19063.

(7) Huang, Y.; Duan, X.; Wei, Q.; Lieber, C.M. Directed Assembly of One-Dimensional Nanostructures into Functional Networks. *Science (80-.).* **2001**, *291* (5504), 630–633.

(8) Zhang, H.; Hussain, I.; Brust, M.; Butler, M. F.; Rannard, S. P.; Cooper, A. I. Aligned Two- and Three-Dimensional Structures by Directional Freezing of Polymers and Nanoparticles. *Nat. Mater.* **2005**, *4* (October), 787–793.

(9) Nørgaard, K.; Weygand, M. J.; Kjaer, K.; Brust, M.; Bjørnholm, T. Adaptive Chemistry of Bifunctional Gold Nanoparticles at the Air/water Interface. A Synchrotron X-Ray Study of Giant Amphiphiles. *Faraday Discuss.* **2004**, *125*, 221–233; discussion 293–309.

(10) Du, J.; O'Reilly, R. K. Anisotropic Particles with Patchy, Multicompartment and Janus Architectures: Preparation and Application. *Chem. Soc. Rev.* **2011**, *40* (5), 2402–2416.

(11) Rodríguez-Fernández, D.; Liz-Marzán, L. M. Metallic Janus and Patchy Particles. *Part. Part. Syst. Charact.* **2013**, *30* (1), 46–60.

(12) Perro, A.; Reculusa, S.; Ravaine, S.; Bourgeat-Lami, E and Duguet, E. Design and Synthesis of Janus Micro- and Nanoparticles. *J. Mater. Chem.* **2005**, *15* (35-36), 3745–3760.

(13) Sam, D. J.; Simmons, H. E. Crown Polyether Chemistry. Potassium Permanganate Oxidations in Benzene. *J. Am. Chem. Soc.* **1972**, *94* (11), 4024–4025.

(14) Lee, K. Y.; Bae, Y.; Kim, M.; Cheong, G.-W.; Kim, J.; Lee, S. S.; Han, S. W. Crown Ether Derivatives-Mediated Self-Assembly of Nanoparticles at the Liquid/liquid Interface. *Thin Solid Films* **2006**, *515* (4), 2049–2054.

(15) Bodnarchuk, M. I.; Yakunin, S.; Piveteau, L.; Kovalenko, M. V. Host–guest Chemistry for Tuning Colloidal Solubility, Self-Organization and

Photoconductivity of Inorganic-Capped Nanocrystals. *Nat. Commun.* **2015**, *6*, 10142.

(16) Gilles, A.; Barboiu, M. Highly Selective Artificial K(+) Channels: An Example of Selectivity-Induced Transmembrane Potential. *J. Am. Chem. Soc.* **2015**, *138*, 426–432.

(17) Sun, Z.; Barboiu, M.; Legrand, Y.-M.; Petit, E.; Rotaru, A. Highly Selective Artificial Cholesteryl Crown Ether K + -Channels. *Angew. Chemie* **2015**, *127* (48), 14681–14685.

(18) Voyer, N.; Arseneault, M.; Otis, F. Synthesis and Characterization of Peptide Nanostructures Designed for Sensing Applications Normand. *Photonic Appl. Biosensing Imaging* **2005**, *5969*, 59690M1–M59690M – 8.

(19) Rasch, M. R.; Rossinyol, E.; Hueso, J. L.; Goodfellow, B. W.; Arbiol, J.; Korgel, B. A. Hydrophobic Gold Nanoparticle Self-Assembly with Phosphatidylcholine Lipid: Membrane-Loaded and Janus Vesicles. *Nano Lett.* **2010**, *10* (9), 3733–3739.

(20) Brust, M.; Fink, J.; Bethell, D.; Schiffrin, D. J.; Kiely, C. Synthesis and Reactions of Functionalised Gold Nanoparticles. *J. Chem. Soc. Chem. Commun.* **1995**, No. 16, 1655–1656.

(21) Cioran, A. M.; Musteti, A. D.; Teixidor, F.; Krpetić, Ž.; Prior, I. A.; He, Q.; Kiely, C. J.; Brust, M.; Viñas, C. Mercaptocarborane-Capped Gold Nanoparticles: Electron Pools and Ion Traps with Switchable Hydrophilicity. *J. Am. Chem. Soc.* **2012**, *134* (1), 212–221.

(22) Bastús, N. G.; Comenge, J.; Puntes, V. Kinetically Controlled Seeded Growth Synthesis of Citrate-Stabilized Gold Nanoparticles of up to 200 Nm: Size Focusing versus Ostwald Ripening. *Langmuir* **2011**, *27* (17), 11098–11105.

(23) Fernández-López, C.; Mateo-Mateo, C.; Álvarez-Puebla, R. A.; Pérez-Juste, J.; Pastoriza-Santos, I.; Liz-Marzán, L. M. Highly Controlled Silica Coating of PEG-Capped Metal Nanoparticles and Preparation of SERS-Encoded Particles. *Langmuir* **2009**, *25* (24), 13894–13899.

(24) Newcomb, C. J.; Sur, S.; Ortony, J. H.; Lee, O.-S.; Matson, J. B.; Boekhoven, J.; Yu, J. M.; Schatz, G. C.; Stupp, S. I. Cell Death versus Cell Survival Instructed by Supramolecular Cohesion of Nanostructures. *Nat. Commun.* **2014**, *5*, 3321.

(25) Pedersen, C. J.; Frensdorff, H. K. Macrocyclic Polyethers and Their Complexes. *Angew. Chem. internat. Ed.* **1972**, *11* (1), 16–25.

(26) Pedersen, C. J. Cyclic Polyethers and Their Complexes with Metal Salts. *J. Am. Chem. Soc.* **1967**, No. I, 2495–2496.

(27) Inokuchi, Y.; Mizuuchi, T.; Ebata, T.; Ikeda, T.; Haino, T.; Kimura, T.; Guo, H.; Furutani, Y. Formation of Host–guest Complexes on Gold Surface Investigated by Surface-Enhanced IR Absorption Spectroscopy. *Chem. Phys. Lett.* **2014**, *592*, 90–95.

(28) Inokuchi, Y.; Ebata, T.; Ikeda, T.; Haino, T.; Kimura, T.; Guo, H.; Furutani, Y. New Insights into Metal Ion–crown Ether Complexes Revealed by SEIRA Spectroscopy. *New J. Chem.* **2015**, *39* (11), 8673–8680.

(29) B. Pullman, N. Goldblum. Metal-Ligand Interactions in Organic Chemistry and

Biochemistry, Part 1. In *Jerusalem Symposia*, ed A. Pullman, N. Goldblum, 1976, pp. 345–349.

(30) Underwood, S.; Mulvaney, P. Effect of the Solution Refractive Index on the Color of Gold Colloids. *Langmuir* **1994**, No. 3, 3427–3430.

(31) Woolley, G. A.; Kapral, M. K.; Deber, C. M. Potential-Sensitive Membrane Association of a Fluorescent Dye. *FEBS Lett.* **1987**, *224* (2), 337–342.

(32) Si, W.; Li, Z. T.; Hou, J. L. Voltage-Driven Reversible Insertion into and Leaving from a Lipid Bilayer: Tuning Transmembrane Transport of Artificial Channels. *Angew. Chemie - Int. Ed.* **2014**, *53* (18), 4578–4581.j

(33) Boal, A. K.; Rotello, V. M. Fabrication and Self-Optimization of Multivalent Receptors on Nanoparticle Scaffolds. J. Am. Chem. Soc., **2000**, **122**, 734–735.

(34) Jackson, A. M.; Myerson, J. W.; Stellacci, F. Spontaneous Assembly of Subnanometre-Ordered Domains in the Ligand Shell of Monolayer-Protected Nanoparticles. *Nat. Mater.* **2004**, *3* (5), 330–336.

(35) Yu, M.; Stellacci, F. Response to "Stripy Nanoparticles Revisited." *Small* **2012**, *8* (24), 3720–3726.

(36) Ong, Q. K.; Reguera, J.; Silva, P. J.; Moglianetti, M.; Harkness, K.; Longobardi, M.; Mali, K. S.; Renner, C.; De Feyter, S and Stellacci, F. High-Resolution Scanning Tunneling Microscopy Characterization of Mixed Monolayer Coated Gold Nanoparticles. *ACS Nano* **2013**, *7* (10), 8529–8539.

(37) Cesbron, Y.; Shaw, C. P.; Birchall, J. P.; Free, P.; Levy, R. Stripy Nanoparticles Revisited. *Small* **2012**, *8* (24), 3714–3719.

(38) Stirling, J.; Lekkas, I.; Sweetman, A.; Djuranovic, P.; Guo, Q.; Pauw, B.; Granwehr, J.; Levy, R.; Moriarty, P. Critical Assessment of the Evidence for Striped Nanoparticles. *PLoS One* **2014**, *9* (11).